1.2a NUMERICAL STUDY OF LOW-LEVEL VORTICITY PRIOR TO TORNADOGENESIS

Scott T. Trevorrow[1], Richard D. Hildner[1], Gregory J. Tripoli[1], Marcus L. Büker[2]

[1]University of Wisconsin – Madison, Madison, Wisconsin
[2]Western Illinois University, Macomb, Illinois

1. INTRODUCTION

In order to investigate the existence of low-level vorticity in pre-tornadogenesis environments associated with the Rear Flanking Downdraft (RFD) of supercell thunderstorms, it has recently been considered useful to look at the orientation and arrangement of vortex lines within a simulated, or observed, domain of interest (e.g. Straka et al. 2007; Markowski et al. 2008; Markowski et al. 2012a, 2012b). Analyses of these lines associated with the cold outflow of the RFD in pre-tornadogenesis environments have shown a consistent trend in their orientation. That is, vortex lines appear to originate near the Rear Flanking Gust Front (RFGF) and arch over the cold pool associated with the RFD (see Markowski et al. 2008). Markowski et al. (2008) proposes that this is evident of the fact that baroclinic production of vorticity is the primary source of low-level rotation, leading up to tornadogenesis, that is then tilted vertically. Specifically, tilting of baroclinically generated vorticity in the RFD via the mesocyclone's main updraft and the region downstream of the main RFD's subsidence core is theorized to instantiate a couplet of cyclonic and anticyclonic vertically oriented vorticity maxima near the ground (Straka et al. 2007; see Fig. 1).

Considering this hypothesis for a moment, it is reasonable to think that the magnitude of baroclinicity and subsidence associated with the RFD is, therefore, proportional to the magnitude of the vertically-oriented vorticity couplet that results at the surface. However, despite the role of the RFD that is recognized to be of critical importance for the development of low-level rotation in environments where there was little initial rotation near the ground (Walko 1993) growing evidence suggests that strong cold pools and strong negative buoyancy near the surface are unfavorable for tornadogenesis (e.g. Markowski et al. 2002; Shabbott and Markowski 2006; Grzych et al. 2007; Marquis et al. 2012). This is a note that Markowski et al. (2008) makes and subsequently suggests that these observations indicate the baroclinicity of the RFD might be a "goldilocks" type of problem, where some baroclinicity is necessary, but too much can result in a rapidly propagating gust front that can, for example, undercut the main updraft (Brooks et al. 1993). The fact that baroclinicity itself has been found to be detrimental to the production of low-level vorticity makes it seem counterintuitive to assume that it is the only crucial RFD characteristic that produces rotation at low levels.

Furthermore, at least to our knowledge, no literature exists showing the evolution of vortex lines (in both simulated and real-world scenarios) that are in contact with the cold pool from their presumed initial horizontal orientation along the leading edge of the cold pool to their arched state. This suggests to us that while the thermodynamically distinct nature of the RFD in contrast with the surrounding low-level environmental air is necessary for the production of low-level rotation, it is not inevitably tilted into the vertical orientation at the scale of vortex line arching.

We instead propose that the horizontal shear across the advancing cold pool (hereafter the advancing cold front will be referred to as the *density current*) is the vorticity observed along the leading edge of the density current that, when evaluating vortex lines in the aforementioned analyses as the process evolves, has an equivalent vortex line arching signature over the cold pool. This perspective explains in a satisfying way why the propagation speed of the density current is important and why vortex lines appear to arch over the cold pool without initially manifesting themselves in a horizontal orientation around the cold pool's leading edge.

In this manuscript, we will show the evolution of low-level vorticity as we have seen it in both idealized and observationally initialized simulations to support the previous accusation while, finally, discussing its relevance and consistency with current research and forecasting tools.

2. METHODOLOGY

The UW Non-hydrostatic Modeling System (UW-NMS), an enstrophy conserving, cloud-resolving, nested grid numerical model (Tripoli 1992) was used to study the evolution of low-level vorticity in simulated, pre-tornadogenesis environments. Two types of simulations were used in this study, the first being an idealized simulation and the second being an observationally initialized simulation.

The idealized simulation was a nested grid simulation of a supercell initialized with a convective bubble in an environment with idealized vertical shear and no topography. The first, most coarse grid, had horizontal resolutions of 3 kilometers and a vertical resolution of 120 meters while covering a domain of nearly 90,000 square-kilometers to a height of roughly 17 kilometers. The first nested grid had horizontal resolutions of 600 meters and a vertical resolution of 120 meters and covered an area of roughly 5,500 square-kilometers to a height of roughly 17 kilometers.

Corresponding author address: Scott T. Trevorrow, Department of Atmospheric and Oceanic Sciences, The University of Wisconsin - Madison, 1225 West Dayton Street Madison, Wisconsin, 53706.
Email: trevorrow@wisc.edu

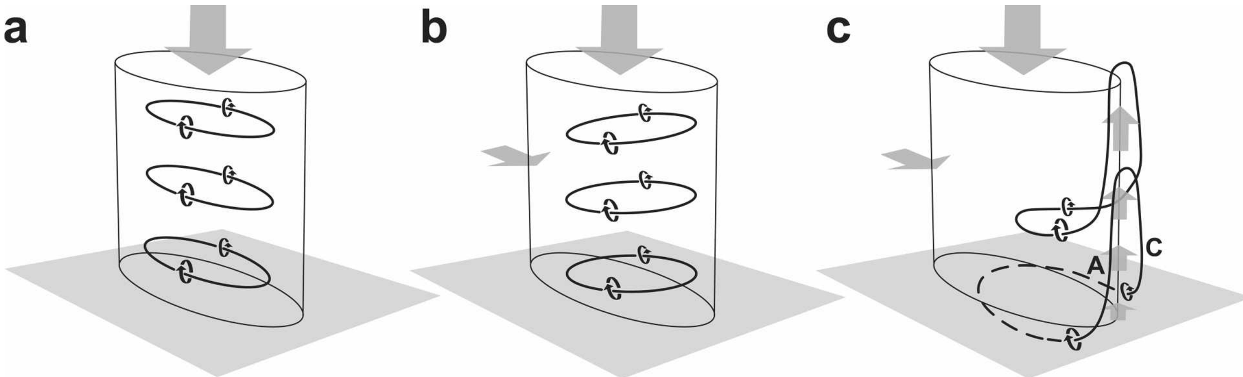

Fig. 1 One possible way by which a couplet of vertical vorticity can be produced by a purely baroclinic process in an environment containing no ambient vorticity (neither vertical nor horizontal). (a) Baroclinically generated vortex rings encircle a buoyancy minimum that extends throughout a vertical column (such a region of negative buoyancy might be found in the hook echo/RFD region of a supercell, for example); the presence of negative buoyancy causes the rings to sink toward the ground as they are generated. (b) If the vortex rings are swept forward as they descend toward the ground owing to the additional presence of rear-to-front flow through the buoyancy minimum, the vortex rings become tilted upward on their downstream sides (a vertical velocity gradient is present within the column because buoyancy is a minimum in the center of the column and increases with increasing distance from the center of the column). (c) If the leading edge of the vortex rings can be lifted by an updraft in close proximity to the buoyancy minimum (an updraft is typically found in close proximity to the hook echo/RFD region of a supercell, for example), then the vortex rings can be tilted further and stretched upward, leading to arching vortex lines and a couplet of cyclonic ("C") and anticyclonic ("A") vertical vorticity that straddles the buoyancy minimum and associated downdraft. Note the similarity to Fig. 15. (Adapted from Straka et al. 2007; Figure caption taken from Markowski et al. 2008)

The second nested grid had horizontal resolutions of 70 meters and a vertical resolution of 120 meters and covered an area of about 450 square-kilometers to a height of about 12 kilometers. The final nested grid (which will hereafter be referred to as the NMS-Id simulation) had horizontal and vertical resolutions of 40 meters and covered an area of roughly 150 square-kilometers to a height of 12 kilometers.

The observationally initialized simulation was a nested grid simulation of a specific tornado-producing mesoscale event (EF-2 event in Goshen County, Wyoming on 5 June, 2009) where the most coarse grid was initialized with observations from the synoptic scale in the form of a GFS analysis 10 hours prior to the storm's initiation. Therefore, the use of the term, "observationally initialized simulation" is not to indicate that it referrers to the use of a data assimilation technique, but rather that the simulation used synoptic scale observation data as an initialization instead of an idealized bubble.

The coarsest grid was centered over Goshen County, Wyoming (105.0°W, 42.0°N) with horizontal and vertical spatial resolutions of 40 kilometers and 200 kilometers respectively while covering an area of roughly 28.8 million square-kilometers to a height of 10 kilometers. A total of four more grids were nested within this grid during the course of the simulation, the first three of which were centered in the exact same geographic location.

The first used horizontal spatial resolutions of 8 kilometers and a vertical resolution of 200 meters over a horizontal area of 4 million square-kilometers to a height of 10 kilometers. The second used horizontal spatial resolutions of 1,600 meters and 200 meters resolution in the vertical which covered a horizontal area of 230,400 square-kilometers to a height of 10 kilometers. The third inner grid began to approach the length scale of the disturbance of interest and thus the grid itself needed to propagate to keep the disturbance in its domain. Therefore, this grid started at 104.3°W, 41.53°N and ended at 104.17°W, 41.426°N. Its horizontal resolution was 320 meters and its vertical resolution was a hybrid of 40 meters resolution for the first 400 meters above ground level and then gradually decreasing to 200 meters resolution at 1 kilometer. The domain of the third inner grid covered an area of roughly 16,000 square-kilometers to a height of roughly only 17 kilometers due to the increased resolution in the vertical. The final nested grid, hereafter referred to as NMS-Ob was a moving grid as well and was centered at 104.3°W, 41.49°N for the initialization and ended at the same location as the previous grid, 104.17°W, 41.426°N. The final inner grid used a horizontal spatial resolution of 64 meters and a vertical resolution of the same sense as the previous third inner grid. Its domain covered an area of roughly 650 square-kilometers to a height of about 17 kilometers.

As the spatial resolutions increased with each grid, so did the temporal resolutions. The first grid was simulated with a time step of 30 seconds, the first inner grid with a time step of 10 seconds, the second inner grid with a time step of 2.5 seconds and the final inner grid with a time step of .625 seconds.

3. SIMULATION RESULTS

3.1 *Idealized Simulation*

First looking at the results of the NMS-Id simulation, Fig. 2a shows the initial existence of a newly formed density current. Its existence is marked by the horizontal equivalent potential temperature gradient at the surface and via the isentropes plotted in the vertical cross section of Fig. 1a which gives the reader a sense of the 3-dimensional geometric shape of the density current. Fig. 1b shows the same oblique view of the identical density current with an isosurface of the magnitude of 3-dimensional vorticity. This isosurface is then colored via the sign of the vertical component of the 3-dimensional vorticity such that warm colors (red) indicate cyclonic vertical vorticity and cool colors (blue) indicate anticyclonic vertical vorticity.

The first noticeable aspect of this image (Fig. 2b) is that there is a sheet of vorticity that arches over, and imitates, the geometric shape of the density current. While it may not be appreciated at the moment, the arched shape of this vorticity sheet will manifest itself in the orientation of developing vortex tubes later in the simulation's evolution. The second most interesting aspect of this image is that along the leading edge of the density current, meaning at the interface between the cold pool and downstream low-level environmental air, there is already vertically oriented cyclonic vorticity. This is to say the horizontal shear across this interface is of large enough magnitude to not only observe it given the chosen 3-dimensional vorticity magnitude isosurface value, but is large enough to account for the majority of the vorticity seen there, hence the solid red coloration of the isosurface. This observation makes it clear that looking solely at the production of horizontal baroclinically generated vorticity via the RFD can be misleading because, although baroclinically produced vorticity is present, it is of far weaker magnitude than the horizontal shear across the leading edge of the density current.

Expanding on the inferred baroclinic production of vorticity for a moment, it is important to note that Fig. 2b does not present the signature of horizontally-oriented vortex rings (or tubes) around the edge of the RFD and density current at low levels, as current theory would suggest. It is also worth mentioning that we are not suggesting these rings are not physically there. As Fig. 2c shows, there is an obvious bulging shape of the vorticity sheet along the leading edge of the same density current when the plotted isosurface value (representing the 3-dimensional vorticity magnitude) is increased. This bulging may very well be associated with a horizontally-oriented vortex tube similar to that suggested by Fujita (1985) when describing downburst processes. However, since there is a hole within the isosurface bulge seen at the density current's leading edge, the magnitude of the vorticity associated with this vortex ring must be far weaker than that of the already present vertically oriented vorticity seen along the interface of the density current and the surrounding low-level environmental air.

Roughly four minutes later, the most interesting development of the vorticity seen on the density current's leading edge occurs. Looking at Fig. 3a, the vorticity sheet breaks down into both vertically oriented vortex tubes along the density current's leading edge that bend back into the cold pool and randomly oriented

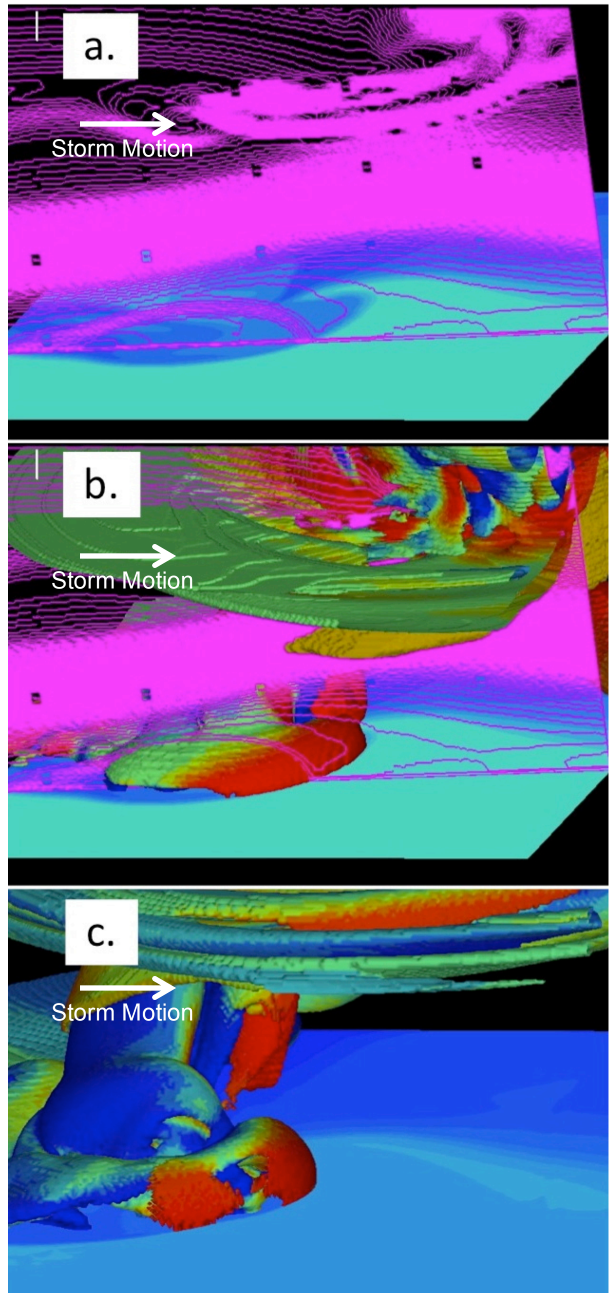

Fig. 2 An oblique view of a storm's density current at time t_0 in the NMS-ld simulation. In all of the images, the colored horizontal cross section shows ground-level equivalent potential temperature, θ_e (*light blue*: warmer, *dark blue:* cooler). (a) A vertical cross section of equivalent potential temperature indicated in the purple isocontours that serves to provide a 3-D perspective of the density current seen in the surface-θ_e horizontal cross-section. (b) Is the same as (a) with the addition of a 3-D isosurface representing the magnitude of 3-D vorticity with a value of .02 s^{-1}. This isosurface is colored by the sign of the 3-D vorticity's vertical component (*red:* cyclonic, *blue*: anticyclonic, *green-yellow*: primarily horizontal). (c) Shows the same type of 3-dimensional isosurface, but the isosurface value is increased to .05 s^{-1}. Notice the bulging shape of the density current's leading edge when the plotted value of vorticity magnitude is increased from .02 s^{-1} in (b) to .05 s^{-1} in (b).

vortex tubes within the cold pool. Notice that the vortex tubes that originate along the leading edge of the density current arch back into the cold pool in the same way the originally observed vortex sheet was arched back, imitating the geometric shape of the density current. What this suggests is that the leading edge of the density current becomes a critical layer in the 3-dimensional flow and the resulting shear instability acts to roll up the sheet of vorticity that was manifested on the density current's leading edge. To more appropriately argue that this is a shear instability rolling up the initial sheet of vorticity, Fig. 3b shows near-surface streamlines in the vicinity of the density current we are interested in. Looking specifically at the region highlighted by the white circle, it is evident that the arched vortex tube associated with this same region in Fig. 3a is the result of the shear line instability manifest in the streamlines of Fig. 3b.

A useful analogy for this process would be to consider a fruit roll-up that has initially been completely unrolled into a fruit sheet. If a stick that is rotating around its long axis is attached to one end of the fruit sheet, the fruit sheet will quickly become coiled up around the rotating stick. Translating this to the process seen from Fig. 2 to Fig. 3, the fruit sheet is analogous to the sheet of vorticity along the leading edge of the density current (Fig. 2b) and the rotating stick is analogous to the shear instability (Fig. 3b). Once the sheet of vorticity on the density current's leading edge breaks down, the resulting shear instability coils up the vorticity sheet in the same sense that the rotating stick coils up the fruit sheet. Fig. 3a presents a nice portrait of this process in the form of a hybrid vortex tube-sheet seen circled in Fig. 3a. The most important thing to recognize, that may not be immediately obvious, is that the result of this sheet roll-up process is not strictly vertically oriented vortex tubes, but arched vortex tubes originating along the density current interface arching back into the cold pool. This is consistent with arched vortex line analyses in current literature, but perhaps more importantly, these arched vortex tubes did not require a vertical tilting mechanism.

In addition to the sheet-roll up process, the interaction between the resulting arched hybrid vortex tube-sheet seen in Fig. 3a and the main updraft of the mesocyclone should not be overlooked. In order to fully appreciate this interaction, it is important to first recognize that the hybrid vortex tube-sheet is arching considerably in the vertical direction, roughly 1.5 kilometers. Secondly, it is important to recognize the spatial orientation of the arched hybrid vortex tube-sheet relative to the main updraft of the mesocyclone. Although not explicitly shown, the main updraft at low-levels is channeled into the cusp of relatively warm-θ_e surface air before turning vertically into the core updraft aloft. While this is a potential reason why at low-levels, specifically near the warm-θ_e cusp, the shear along the density current interface becomes unstable, it is also important because once the sheet roll-up process starts, the updraft and arched hybrid vortex tube-sheet are reasonably co-located. Therefore, updraft stretching of this arched vortex tube-sheet acts to tighten the vortex tube due to angular momentum conservation which, in turn, enhances convergence near the base of the tube, consequently enhancing the sheet roll-up process.

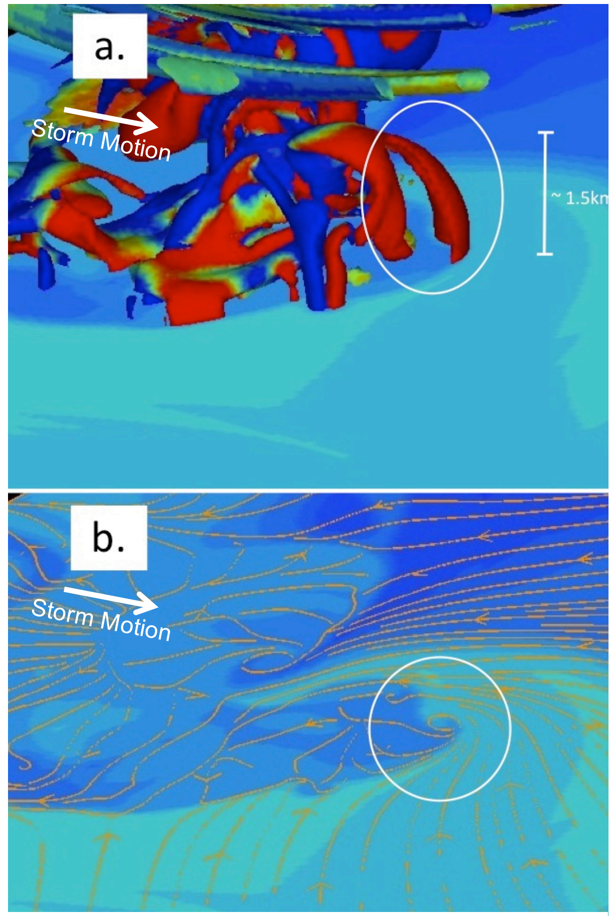

Fig. 3 An oblique view of the vortex sheet roll-up process at t_0 + 4 minutes into the NMS-ld simulation. The horizontal cross section in both (a) and (b) shows surface-level equivalent potential temperature, θ_e (*light blue*: warmer, *dark blue:* cooler). (a) Shows a 3-dimensional isosurface which represents the 3-D vorticity magnitude of .05 s^{-1} and is colored by the sign of the vertical component of vorticity (*red:* cyclonic, *blue*: anticyclonic, *green-yellow*: primarily horizontal). The white oval seen in (a) is used to draw the reader's attention to the arched hybrid vortex tube-sheet it encircles. This hybrid tube-sheet manifests the sheet roll-up process described in the text. The vertical scale bar in (a) next to the white oval is used to give a perspective on the height of this arched hybrid tube-sheet, roughly 1.5 kilometers. (b) Stripping away the 3-dimensional isocontour and plotting surface streamlines allows us to conclude that the hybrid vortex tube-sheet in (a) is the result of a shear instability along the density current's leading edge as seen by the instability circled in (b). Notice that this looks like a Kelvin-Helmholtz instability.

The result of this sheet roll-up enhancement can be seen in Fig. 4 where the white arrow indicates updraft stretching of the arched vortex tube-sheet previously seen in Fig. 3a. At this point, roughly four minutes further into the simulation from Fig. 3, what was once an arched hybrid vortex tube-sheet (Fig. 3a) has now strengthened and stretched such that it is a

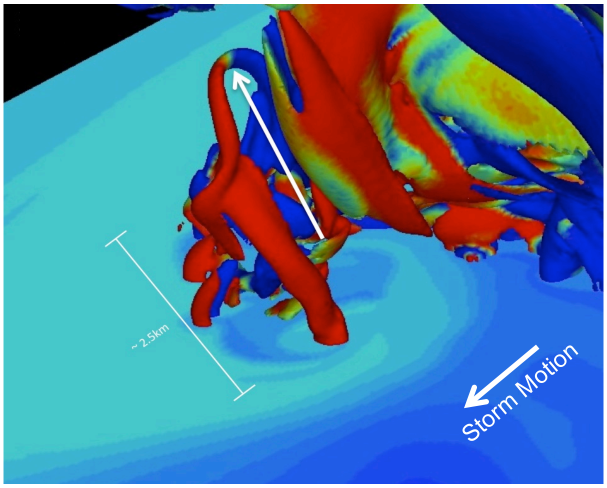

Fig. 4 An oblique view of the arch stretching process as a result of the arched vortex tube's interaction with the mesocyclone updraft at t_0 + 8 minutes into the NMS-Id simulation. Notice from Fig. 2 and Fig. 3 this figure has rotated counter-clockwise roughly 90°. The horizontal cross section shows surface-level equivalent potential temperature, θ_e (*light blue*: warmer, *dark blue:* cooler), and the 3-D isosurface shows the 3-D vorticity magnitude of .05 s^{-1} that is then colored by the sign of the vertical component of vorticity (*red:* cyclonic, *blue*: anticyclonic, *green-yellow*: primarily horizontal). The white arrow is used to indicate the region of arch stretching by the mesocyclone updraft, while the vertical scale bar is used to give the reader a perspective of the height of the arch at this time (roughly 2.5 kilometers) compared to the previous time in Fig. 3b (roughly 1.5 kilometers). Notice that what once was a hybrid vortex tube-sheet has now become a prominent vortex funnel and there is relatively little of the vortex sheet that was seen in Fig. 2b remaining in close proximity to the funnel.

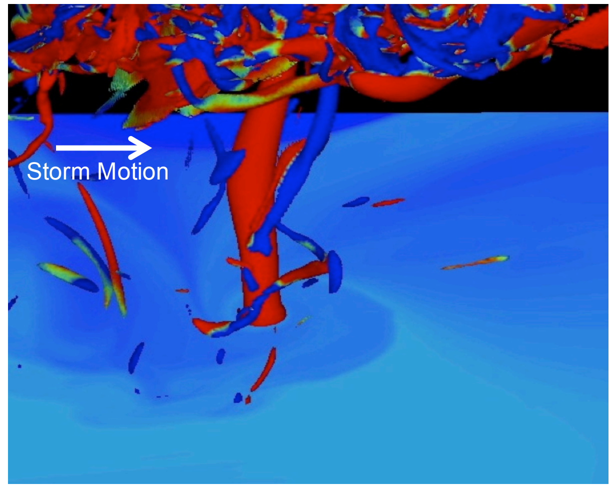

Fig. 5 An oblique view (now rotated back to the original angle of view, 90° clockwise from Fig. 4) of a mature vortex funnel at t_0 + 20 minutes into the NMS-Id simulation that has stretched vertically enough, via the mesocyclone's updraft, to connect with the mesocyclone vorticity at mid-levels. The horizontal cross section shows surface-level equivalent potential temperature, θ_e (*light blue*: warmer, *dark blue:* cooler) and the 3-dimensional isosurface shows the 3-dimensional vorticity magnitude of .05 s^{-1} that is then colored by the sign of the vertical component of the 3-dimensional vorticity (*red:* cyclonic, *blue*: anticyclonic, *green-yellow*: primarily horizontal). Notice that there is no longer any shear associated with the leading edge of the cold pool since the strong central funnel's circulation has consolidated all of the previously seen low-level vorticity associated with the density current into itself.

---

cyclonically rotating vortex tube that still arches back into the cold pool. Notice there is relatively little of the vortex sheet remaining in the area closest to the strong vortex funnel, manifesting the previously described sheet-rolling enhancement process. Considering the spatial orientation of the updraft and the shape of density current interface, it is perhaps not a coincidence why the initial break-down of the vortex sheet occurred in a region of close proximity to the low-level, warm θ_e cusp. Both flow channeling into the warm θ_e cusp and the cyclonically-curved shape of the density current in this region aid in strengthening the vorticity along the leading edge of the density current at this location, ultimately resulting in the instability seen in Fig. 3b.

Finally, after twelve minutes of this roll-up process, the resulting funnel is connected with the mid-level vorticity associated with the mesocyclone and is the center of its own cyclonic circulation near the ground. This is evident because, although there is still baroclinicity associated with the cold pool in the low-level environment evident by the ground-level θ_e in Fig. 5, there is no vorticity along the cold pool's leading edge.* The strong funnel is, therefore, completely exhausted of its low-level vorticity input and is solely dependent on its connection with the mid-level vorticity associated with the mesocyclone for further maintenance.

3.2 *Observationally Initialized Simulation*

Comparing the results of the idealized simulation (NMS-Id) with those of the observationally initialized simulation (NMS-Ob) shows the equivalent stretching process of a vortex tube that is initially arched over the storm's density current from interaction with the mesocyclone's main updraft. Fig. 6a shows the cold pool that is associated with the storm's RFD via a vertical cross section of equivalent potential temperature and streamlines. Fig. 6b shows the 3-dimensional magnitude of vorticity associated with the leading edge of the density current via a 3-dimensional isosurface colored in the same way as the NMS-Id simulation analyses; red indicates cyclonic vertical vorticity and blue indicates anticyclonic vertical vorticity. Since there is a signature of vorticity associated with the leading edge of the cold pool, it must have some magnitude of storm relative motion and will, therefore, be referred to

*Notice we refer to the relatively cool θ_e region as the "cold pool" as opposed to the "density current" since at this time there is no storm-relative advancement of the cold pool. Hence the lack of substantial vorticity along its leading edge.

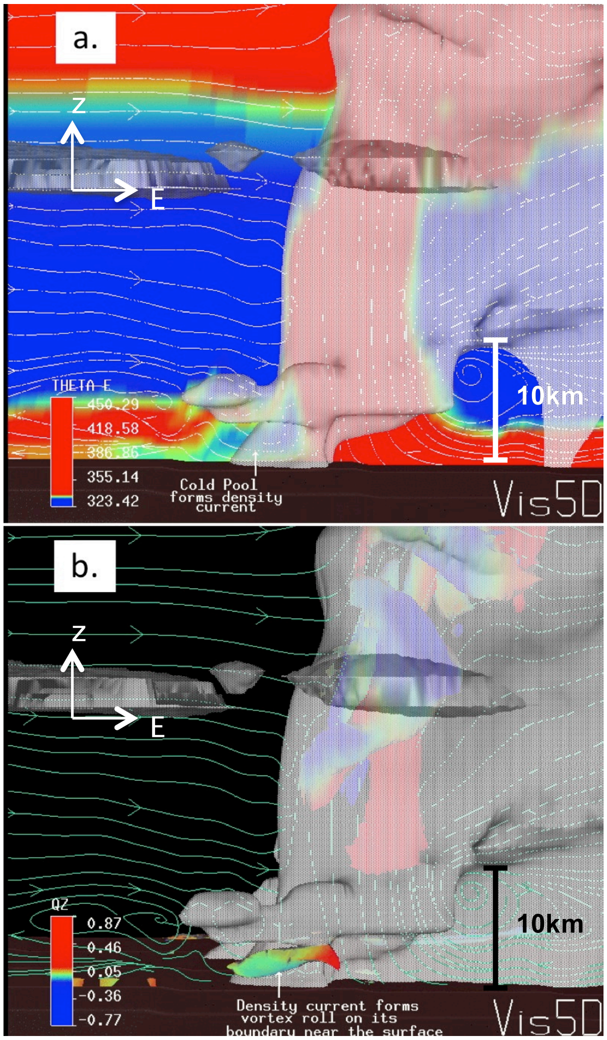

Fig. 6 The results of the NMS-Ob simulation at time t_0, looking North. (a) The colored vertical cross section shows the vertical distribution of equivalent potential temperature (θ_e) with streamlines and the white 3-D isosurface is the storm's cloud mass. Here the reader should recognize the cold pool's orientation for reference in (b). (b) The vertical cross section of θ_e has been stripped away and another 3-D isosurface has been added that shows the magnitude of the 3-D vorticity with a value of .4 s^{-1}. This is then colored by the sign of the 3-D vorticity's vertical component (*red:* cyclonic, *blue*: anticyclonic, *green-yellow*: primarily horizontal). Notice that there already exists an arched vortex tube along the leading (eastward) edge of the density current, nearly underneath the updraft.

from now on as the storm's density current.

Continuing to focus on Fig. 6b for a moment, at this point in the simulation the sheet of vorticity along the leading edge of the density current has already rolled up into a primary arched vortex tube that imitates the geometric shape of the density current seen in Fig. 6a. This corresponds with Fig. 3a of the NMS-Id simulation not only due to the existence of similarly arched vortex tubes, but due to the fact that the end of the vortex tube in contact with the leading edge of the density current in Fig. 6a of the NMS-Ob simulation is also vertically oriented and cyclonically rotating. Finally, it is also comparable to Fig. 3a of the NMS-Id simulation in that the arched vortex tube seen in Fig. 6a is nearly vertically juxtaposed with the main updraft of the mesocyclone.

Two minutes later in the simulation, the arched vortex tube is stretched vertically which is manifest in the enhanced arch shape of the tube in Fig. 7a. This response to the mesocyclone's updraft is continued as the simulation evolves and the resulting rotational enhancement extends the vorticity at the base of the vortex tube all the way to the ground (Fig. 6b). Ten minutes further into the simulation, the vortex tube continues to be stretched vertically via the updraft and ultimately connects with the mid-level vorticity associated with the mesocyclone (Fig. 6c).

At this point, one may ask why there was no obvious indication of a sheet roll-up process in the NMS-Ob simulation prior to the observed stretching process. It is important to point out that, although the illustrated stretching process observed in the NMS-Ob simulation analysis appears to be similar to that of the NMS-Id simulation, the resolution and scale of the NMS-Ob simulation is coarser and much larger than that of the NMS-Id simulation. Therefore, the small scale roll-ups of the vorticity sheet seen in the NMS-Id simulation (Fig. 3a) are too small, relative to the scale of the NMS-Ob grid, to be plotted cleanly. It is still encouraging, however, to see that once the arched vortex tubes are initiated, interaction with the mesocyclone's main updraft results in vertical stretching of the same arched vortex tubes in more than one simulated case. Nevertheless, we recognize the importance of studying the NMS-Ob simulation with finer resolution to see if the same sheet roll-up process observed in the NMS-Id simulation is observed in the NMS-Ob simulation. This is an intended area of further investigation prior to publication of this study.

4. DISCUSSION AND CONCLUSION

This manuscript has shown that, in an idealized simulation, the strongest signature of the vorticity associated with a supercell's density current is in the form of a vorticity sheet that imitates the geometric shape of the density current (Fig. 2a). Specifically, the horizontal shear along the leading edge of the density current (which is also the leading edge of the previously mentioned sheet of vorticity) manifests itself as vertically oriented cyclonic vorticity. Once the density current's leading edge becomes a critical layer in the 3-dimensional flow, the resulting shear instability rolls up the sheet of vorticity into a vortex tube that still imitates the geometric shape of the density current and, thus, appears arched (Fig. 3a). This arched vortex tube, if both close enough to the region of low-level air ingestion at the base of the mesocyclone's updraft and tall enough to be influenced by the rising motion of low-level air into the updraft, is then vertically stretched. This stretching process was seen in both our simulated and observationally initialized simulations (Fig. 4a, Fig. 7a,b,c). Stretching of the arched vortex tube ultimately results in an enhancement of the sheet-roll up process until the vortex tube consolidates all of the vorticity

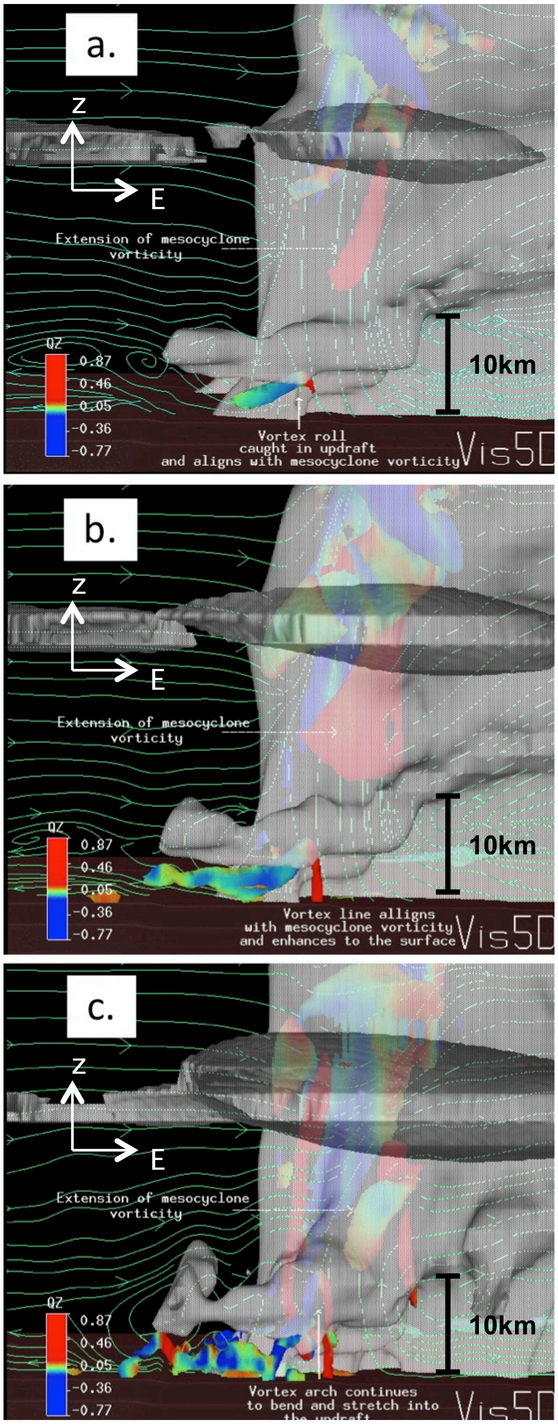

Fig. 7 Looking North, a vertical cross section of streamlines is plotted against a white 3-D isosurface representing the storm's cloud mass and a 3-D isosurface showing the magnitude of 3-D vorticity with a value of .4 s^{-1}, colored by the sign of the 3-D vorticity's vertical component (*red:* cyclonic, *blue*: anticyclonic, *green-yellow*: primarily horizontal) at (a) t_0 + 2 minutes, (b) t_0 + 4 minutes and (c) t_0 + 15 minutes into the NMS-Ob simulation. Notice that as the mesocyclone's updraft stretches the arched vortex tube into the mesocyclone, the vorticity of the tube is subsequently enhanced until it extends to the surface.

associated with the density current (Fig. 5). At this point, the arched vortex tube has no source of low-level vorticity for further development, but is stretched vertically enough to rely on the vorticity of the mesocyclone at mid-levels for further maintenance.

The existence of arched vortex tubes in our idealized and observationally initialized simulations is consistent with current literature showing the same existence of arched vortex lines in simulated and real-world pre-tornadogenesis environments (Markowski et al. 2008; Markowski et al. 2012a,b). However, the fact that the vorticity along the leading edge of the density current in our simulations is initially vertically oriented cyclonic vorticity and initially extends to the surface is in contrast with the current perspective that the dominating vorticity feature associated with a supercell's Rear Flanking Downdraft (RFD) and density current is horizontally-oriented vortex rings that surround the RFD and density current, much like a Fujita (1985) vortex ring appears in his analysis of a downburst.

The significance of concluding that the shear across the interface between the leading edge of the density current and surrounding low-level environmental air is the important low-level vorticity associated with the density current in pre-tornadogenesis environments as opposed to baroclinically generated horizontally-oriented vorticity is three-fold.

1.) As stated in (1) and (3), the shear perspective presented in this manuscript requires no vertical tilting mechanism to re-orient baroclinically generated horizontally-oriented vorticity associated with the RFD and density current. This is significant since, to our knowledge, there is no literature to-date that physically shows, through simulation or observation, the process of tilting horizontally-oriented vorticity into the vertical.
2.) It explains why the strength of a storm's cold pool and the propagation speed of the associated density current have been found to be detrimental to tornadogenesis (e.g. Grzych 2007). Although it wasn't explicitly discussed in this manuscript, it is easy to reason that the sign of the shear across the leading edge of the density current depends on the relative magnitudes of both the density current's propagation and surrounding low-level environmental flow. Specifically considering a situation where there exists strong environmental southerly flow at low-levels, it is easy to imagine that given a gentle eastward propagating density current in this environment, there will be cyclonic horizontal shear along the leading (eastward) edge of the density current. Augmenting the same thought experiment with strong southerly flow at low-levels, the conclusion can be made that the stronger the low-level southerly flow, the faster a density current can propagate eastward without changing the sign of the shear along its leading edge. An equivalent thought experiment can be done for situations where the shear on the leading edge of the density current is anticyclonic, in which case the sheet roll-up process we discussed in this manuscript is impossible to achieve. These

thought experiments are not limited to strictly southerly low-level flow and eastward propagating density currents as well. Although we submit that the previous explanation is pure reasoning without experimental evidence, we have subtly stumbled upon one of the most exciting theoretical conclusions of our research. The fact that the low-level environmental flow is an important variable in determining whether or not the observed sheet roll-up process (and ultimately tornadogenesis) will occur is consistent with the recognized importance of looking at low-level (0-1 kilometer) environmental shear for predicting a supercell's tornado potential (e.g. Thompson et al. 2003; Craven and Brooks 2004).

3.) It is consistent with current research investigating tornado maintenance (Marquis et al. 2012). Considering that in Fig. 5 we observed a central funnel exhausted of its supply of low-level vorticity, it is reasonable to assume that an additional pulse of the RFD would act to provide another source of low-level vorticity which can then be aggregated into the main funnel via the equivalent sheet roll-up process we observed at a previous time in the simulation. Since a pulse of the RFD would, in effect, advance the cold pool relative to the storm, there would again be shear across the interface between the leading edge of the density current and surrounding low-level environmental air. This is a parallel conclusion with Marquis et al. (2012) who concluded that new density current surges after tornadogenesis appear to assist in tornado maintenance. Although, Marquis et al. (2012) continues to suggest that the new surges of cold outflow associated with the density current aid tornado maintenance by baroclinically producing, and subsequently tilting, horizontal vorticity. This is in obvious contrast with our explanation.

While this perspective on low-level vorticity prior to tornadogenesis presents exciting parallels with current research, the authors of this manuscript still intend to investigate these connections explicitly. In addition, an analysis of the observationally initialized simulation representing the Goshen County, Wyoming tornado-producing event at higher resolution and finer scales is needed in order to establish a relationship with the sheet roll-up process observed in the idealized simulation. The authors of this paper also intend to investigate how this process of tornadogenesis is connected to the top-down transport of mid-level baroclinically generated vorticity.

5. ACKNOWLEDGEMENTS

This research was supported by the National Science Foundation (NSF) grant number AGS-1137137.

REFERENCES

Brooks, H. E., C. A. Doswell III, and R. P. Davies-Jones, 1993: Environmental helicity and the maintenance and evolution of low-level mesocyclones. *The Tornado: Its Structure, Dynamics, Prediction, and Hazards, Geophys. Monogr.*, Vol. 79, Amer. Geophys. Union, 97–104.

Craven, J. P., and H. E. Brooks, 2004: Baseline climatology of sounding derived parameters associated with deep, moist convection. *Natl. Wea. Dig.,* **28**, 13–24.

Fujita, T. T., 1985: The downburst. Satellite and Mesometeorology Research Project, University of Chicago, 122 pp.

Grzych, M. L., B. D. Lee, and C. A. Finley, 2007: Thermodynamic analysis of supercell rear-flank downdrafts from Project ANSWERS. *Mon. Wea. Rev.*, **135**, 240–246.

Markowski, P. M.,, J. M. Straka, and E. Rasmussen, 2002: Direct surface thermodynamic observations within the rear-flank downdrafts of nontornadic and tornadic supercells. *Mon. Wea.Rev.,* **130**, 1692–1721.

——, E. N. Rasmussen, J. M. Straka, R. P. Davies-Jones, Y. Richardson, and J. Trapp, 2008: Vortex lines within lowlevel mesocyclones obtained from pseudo-dual-Doppler radar observations. *Mon. Wea. Rev.*, **136**, 3513–3535.

——, Y. Richardson, J. Marquis, R. P. Davies-Jones, J. Wurman, K. Kosiba, P. Robinson, E. N. Rasmussen, and D. Dowell, 2012a: The pretornadic phase of the Goshen County, Wyoming, supercell of 5 June 2009 intercepted by VORTEX2. Part I: Evolution of kinematic and surface thermodynamic fields. *Mon. Wea. Rev.,* **140**, 2887–2915.

——, Y. Richardson, J. Marquis, R. P. Davies-Jones, J. Wurman, K. Kosiba, P. Robinson, E. N. Rasmussen, and D. Dowell, 2012b: The pretornadic phase of the Goshen County, Wyoming, supercell of 5 June 2009 intercepted by VORTEX2. Part II: Intensification of Low-level Rotation. *Mon. Wea. Rev.,* **140**, 2916-2938.

Marquis, J., Y. Richardson, P. M. Markowski, D. Dowell, and J. Wurman, 2012: Tornado maintenance investigated with high-resolution dual-Doppler and EnKF analysis. *Mon. Wea. Rev.*, **140**, 3–27.

Shabbott, C. J., and P. M. Markowski, 2006: Surface in situ observations within the outflow of forward-flank down drafts of supercell thunderstorms. Mon. Wea. Rev., 134, 1422–1441.

Straka, J. M., E. N. Rasmussen, R. P. Davies-Jones, and P. Markowski, 2007: An observational and idealized numerical examination of low-level counter-rotating vortices toward the rear flank of supercells. *Electron. J. Severe Storms Meteor.,* **2**, 1–22.

Thompson, R. L., R. Edwards, J. A. Hart, K. L. Elmore, and P. M. Markowski, 2003: Close proximity soundings within supercell environments obtained from the rapid update cycle. *Wea. Forecasting*, **18**, 1243–1261.

Tripoli, G. J., 1992: A Nonhydrostatic Mesoscale Model Designed to Simulate Scale Interaction. *Mon. Wea. Rev.*, **120**, 1342–1359.

Walko, R. L., 1993: Tornado spin-up beneath a convective cell: Required basic structure of the near-field boundary layer winds. *The Tornado: Its Structure, Dynamics, Prediction, and Hazards, Geophys. Monogr.*, Vol. 79, Amer. Geophys. Union, 89–95.